Supporting Information

Shapiro et al. 10.1073/pnas.1323094111

SI Materials and Methods

Coral Species and Growth Conditions. Small colonies of the coral *Pocillopora damicornis*, obtained from the Birch Aquarium at Scripps, were kept in aquaria at 25 °C in artificial seawater (Instant Ocean; Spectrum Brands Company) on a 12-h light–dark cycle. A *Favia* colony was obtained from a supplier of aquarium needs (Drs. Foster & Smith). Fragments of *Acropora* sp., *Montipora* sp., and *Seriatopora histrix* colonies as well as colonies of the Zoanthids *Protopalythoa* sp. and *Palythoa* sp. and polyps of a *Discosoma* sp. were obtained from the ProReef Coral Aquaculture Facility (Naan, Israel). A fragment of Red Sea *Stylophora pistillata* was obtained from the laboratory of Oren Levi (Bar Ilan University, Ramat-Gan, Israel).

Coral Explants. Coral explants were obtained as follows. Small fragments of a *P. damicornis* branch were crushed using clean pliers, washed in a Petri dish filled with 50 mL filter-sterilized artificial seawater (FASW), and transferred to a covered Petri dish for incubation on a rotary shaker (50 rpm) at 25 °C with a 12-h light–dark cycle. Fragments were checked on a daily basis for the release of viable tissue explants. Explants of 0.5- to 1-mm diameter were collected using a clean glass pipette and transferred to a Petri dish containing FASW under identical incubation conditions, where they could be maintained for several days (Figs. 1*A* and 2 *A* and *C*).

Microscopy. All light microscopy was performed using a Nikon Ti inverted microscope, with the exception of the light microscopy shown in Fig. S2 *A–D*, which was captured using an Olympus IX81 microscope. EM was performed using a Carl Zeiss Ultra 55 scanning electron microscope.

Electron Microscopy. Small fragments of *P. damicornis* were anesthetized by gradual addition of a $MgCl_2{\cdot}6H_2O$ solution in FASW to a final concentration of 40 mg/mL. Samples were fixed with 2% (vol/vol) paraformaldehyde and 3% (vol/vol) glutaraldehyde in FASW. After fixation, samples were washed three times for 15 min in FASW followed by double-distilled water. Samples were then dehydrated in ascending concentrations [50–100% (vol/vol)] of ethanol and dried in a BAL-TEC CPD 030 Critical Point Drier. Dehydrated samples were placed on carbon tape and sputter-coated with gold palladium (S150; Edwards) before imaging (Fig. 2*B*).

Flow-Field Analysis. Each video of the tracer particle motion was converted to a sequence of differences between subsequent frames to focus on motion and eliminate stationary features from subsequent analysis (Fig. 1 *B* and *C*). The instantaneous velocity of tracer particles was determined using an in-house tracking algorithm implemented in Matlab (The MathWorks). The resulting data were used to generate a map of flow velocities by dividing the field of view into 21 × 21-μm squares and calculating the median velocity over the duration of the video in each square. This raw velocity map was smoothed using a 3 × 3 2D median filter and then resampled to the initial image resolution (4.25-μm grid) by linear interpolation.

Fig. 1 *B* and *C* show composite images displaying the 2D velocity field in the context of the flow field (streaklines) and the coral surface. Streaklines represent the particle traces and were obtained from the same video used to generate the velocity field after taking the difference between consecutive frames and then computing the maximum intensity projection (a single image generated from a video sequence, where the intensity of each pixel is set to the maximum value that that pixel achieves over the entire sequence). Streaklines were made transparent using image processing software (GNU Image Manipulation Program GIMP 2.8) and superimposed on the color-coded velocity field. Additionally, a single raw frame from the video was overlaid and masked so that only the coral remained visible to show the flow in the context of the coral surface and, particularly, the polyp locations.

Oxygen Microelectrodes. Local dissolved oxygen concentrations were measured using OX25 or OX50 oxygen microelectrodes (Unisense) connected to an OXY-meter amplifier and recorded using the SensorTrace-PRO software (Unisense). Before each experiment, electrodes were calibrated linearly using readings in oxygen-free water, where oxygen had been scavenged by the addition of sodium sulfite (Na_2SO_3), and air-saturated FASW (0.2 μm) of known salinity and temperature (Fig. 3).

Simultaneous Flow-Field Imaging and Oxygen Measurements. For Fig. 3 *A* and *B*, the concentrations from a single profile are superimposed on a maximum intensity projection of the flow field captured immediately before oxygen measurements, with a single raw image from the video overlaid and masked to only show the coral. For Fig. 3*C*, a 2D oxygen map was composed of 11 profiles obtained as above and space of 100 μm between them. The resulting oxygen concentration matrix was up-sampled fourfold and smoothed using a Gaussian filter with a 50-μm standard deviation. Fig. 3*C* was then generated using the same procedure as for Fig. 1 *B* and *C*, described above, with the oxygen concentration map replacing the velocity map.

All dissolved oxygen concentrations are presented as percentages of the ambient dissolved oxygen concentration, where it was taken as the average of the first five measurements of each profile (i.e., from 2,100 to 2,500 μm from the coral surface of the first profile). For Fig. 3*C*, concentrations were normalized to the ambient concentration of the first profile.

Oxygen Measurements in the Absence of Ciliary Beating. Ciliary action was arrested by incubating a coral branch for 10–15 min in FASW supplemented with 0.1 mM sodium orthovanadate (Na_3VO_4; New England BioLabs). After confirming by microscopic observation and video analysis that ciliary beating had stopped, dissolved oxygen measurements were performed as described above.

Mathematical Model of Mass Transport. The numerical investigation of the effect of vortical ciliary flows on mass transport, carried out in COMSOL Multiphysics, version 4.2.a (COMSOL Inc.), consisted of four coral morphotypes.

Small-polyped branch. This geometry was most directly modeled after the cross section of a branch of *P. damicornis* and the observed ciliary flows. The coral consists of a smooth 5-mm-diameter disk within a 100 × 120-mm simulation domain. The tangent velocity boundary condition imposed on the branch circumference is shown in Fig. S4*B*: the boundary forcing was sinusoidal, with the period set to eight full cycles (1.96-mm period), resulting in 0.98-mm-wide vortices (Fig. S4 *A* and *B*).

Small-polyped plate. This geometry captures the surface characteristics of the small-polyped branch without the form (i.e., cylinder) factor. It can be considered representative of a plating colony with similar polyp geometry and ciliary forcing to *P. damicornis*. This geometry also isolates the interaction between ciliary flows and

the boundary layer by avoiding flow elements, such as the wake and upstream stagnation point occurring in the branch geometry. The coral consists of a smooth 70-mm-long section of the lower boundary of the 80 × 50-mm simulation domain. On this section, a sinusoidal 2-mm-period tangential velocity forcing is applied. On either side of the forced section, there is a 4-mm length of no-slip buffer region (Fig. S4 *C* and *D*) (i.e., a ciliary flow-free region). The remaining sections of the horizontal boundary have slip conditions and thus, do not contribute to the boundary-layer formation.

Large-polyped mound. This geometry addresses the question of whether the surface topology associated with larger-polyped corals, such as *F. fragum*, interferes with the ciliary mixing. The mounding colony is modeled as a 45-mm-diameter half-disk protruding from a flat, no-slip surface representing the ground, and enclosed within a 120 × 50-cm simulation domain. The coral has 2-mm-deep trapezoidal indentations along its surface that model the cavities (corallites) in which polyps reside (Fig. S4 *E* and *F*). The interpolyp ridges (coenestea) are 2 mm long, whereas corallites are 3 mm in diameter with 0.7-mm sloping transitions. The direction of flow relative to the polyp surface structure was modeled after previous observations (1, 2) showing that ciliary currents are directed radially from the center of the polyp. To represent this flow pattern, a smooth square wave was used with 0.2-mm-long sinusoidal transitional regions (Fig. S4*F*), resulting in a vortex width of ∼3.2 mm. The entire lower boundary of the domain has a no-slip condition, representing the ground. The model further assumed that the boundary layer over the ocean floor had grown for ∼50 cm by the point that it reached the colony. This length is sufficient for a substantial boundary layer–mound interaction at all of the ambient flow velocities examined.

Large-polyped plate. This geometry uses the same trapezoidal polyp structure as in the mounding colony but on a flat surface, with the goal of removing the form (i.e., half-disk) factor. It can be considered broadly representative of an encrusting colony of *F. fragum*. The cavities (corallites) of the large polyps recede into the boundary of the 80 × 50-cm field. The coral section is 70.4 mm of polyp cavities and ridges, with a small length (7.4 mm) of no-slip boundary on either end (Fig. S4*G*).

To examine the interaction between ciliary flows and ambient flow, unidirectional ambient flow was imposed, and its velocity varied between 10 μm s^{-1} and 10 mm s^{-1}. The two plate geometries were simulated up to an ambient flow velocity of 50 mm s^{-1}, still below the transition to a turbulent boundary layer. A separate transient simulation of the coral branch geometry was performed to examine the effect of higher ambient flow velocity (50 mm s^{-1}), which falls in the unsteady vortex shedding regime (blue circle in Fig. 5*B*). Twenty seconds were simulated to allow sufficient time for the stabilization of the flow and oxygen flux.

Oxygen production was modeled by a constant concentration on the coral surface—equal to two times the ambient concentration—of a solute with diffusivity of 2×10^{-9} m^2 s^{-1}. This constant concentration boundary condition models the condition when oxygen buildup in the coral tissue regulates oxygen production. Under these conditions, the steady-state flux of oxygen from the surface can be integrated and compared with the case without cilia (the latter corresponding to a no-slip flow boundary condition on the branch surface) as in Fig. 5*B*. A transient simulation of the sudden onset of oxygen production in a steady 0.1-mm s^{-1} ambient flow for the branch geometry was used to compare oxygen distributions between the numerical simulation (Fig. 4) and the experimental observations (Fig. 3). The transience in oxygen production captures the inherent unsteadiness in the coral, and the transects in Fig. 4 correspond to 1 min after production begins.

High-Resolution Imaging of Vortical Ciliary Flows. Ciliary flows over small segments of detached coral tissue (coral explants; see above) were visualized by tracing the motion of polystyrene tracer particles (1-μm diameter; Thermo Scientific) in the surrounding water (Fig. 2*A* and Movies S2 and S3). Visualization was performed in chambers prepared as follows. A 1 × 2-cm strip of double-sided adhesive tape was attached to the surface of a 24 × 60-mm glass coverslip. A rectangular section was cut from the center of the adhesive tape using a clean scalpel to create a shallow well ∼100 μm in depth. A single explant was transferred to the chamber together with a dilute suspension of polystyrene tracer particles in FASW, and the chamber was sealed by gently pressing a second glass coverslip on top. Cilia and particle motion were visualized by phase-contrast microscopy (100×, 1.4 N.A. objective) and captured using a Photron SA-3 high-speed camera (17 μm/pixel) at up to 1,000 frames per second.

High-Resolution Analysis of Vortical Ciliary Flows. The motion of the tracer particles in the high-resolution videos was tracked using an in-house, semiautomated, predictive particle tracking algorithm, with 1-pixel accuracy, implemented in Matlab (Fig. 2*A* and *C* and Movies S2 and S3). The high frame rate allowed us to capture oscillations in the tracer motion caused by ciliary beating, and trajectories were smoothed using a second-order Savitsky–Golay filter with a five-frame window. The 2D slice of the velocity field near the coral surface (Fig. 2*A*) was generated from the particle tracks by dividing the field of view into 8.7 × 8.7-μm squares and computing the mean tracer velocity in each square over the entire duration of the video (∼5,500 frames). Linear interpolation was used to fill in the few grid points where information was missing because of low tracer seeding. The profile of the surface-parallel flow velocity as a function of distance from the coral surface (Fig. 2*B*) was generated from the same data: in this case, the surface-parallel component of the tracer velocity was binned in 1.87-μm increments of distance from the coral surface and averaged over the field of view shown in Fig. 2*A*. The ciliary beating pattern (Fig. 2*C*, *Inset* and Movie S3) was obtained by tracking one cilium manually (through the identification of 25 points on the cilium in each frame) over five full beat cycles at 500 frames per second under identical imaging conditions as those above. The shape of the tracked cilium was smoothed using a second-order Savitsky–Golay filter with a five-point window.

1. Lewis JB, Price WS (1976) Patterns of ciliary currents in Atlantic reef corals and their functional significance. *J Zool* 178(1):77–89.

2. Yonge CM (1930) Studies on the physiology of corals. I. Feeding mechanisms and food. *Great Barrier Reef Expedition 1928-29, Scientific Reports* [British Museum (Natural History), London, UK], pp 13–57.

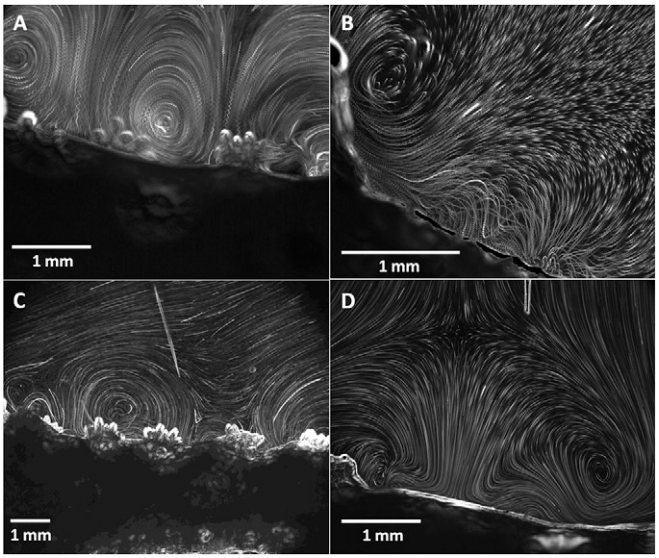

Fig. S1. Vortical flow on four *P. damicornis* fragments under different observation conditions. (*A*) Fragment held at the center of an open Petri dish (depth of 5 mm and diameter of 40 mm). The imaging plane was ~2 mm above the bottom surface. Zig-zag patterns in particle trajectories are caused by slight vibrations from the free surface. (*B*) Similar to *A* but with the fragment suspended so that the imaging plane is more than 3 mm above the bottom surface. (*C*) Fragment held in a semienclosed 5-mm-deep chamber as described for microelectrode experiments. The imaging plane was ~2 mm above the bottom of the chamber. The larger field of view (because of lower magnification) shows six polyps and multiple vortices along the fragment edge. The tip of the microelectrode is seen at the top of the image. (*D*) Same setting as in *C*. The image shows particles next to the surface flowing in opposite directions, thus creating the fundamental element of the repeating vortex pattern, namely two opposing vortices. All panels are maximal intensity projections from videos captured by dark-field microscopy using either a (*C*) 2× or (*A*, *B*, and *D*) 4× objective.

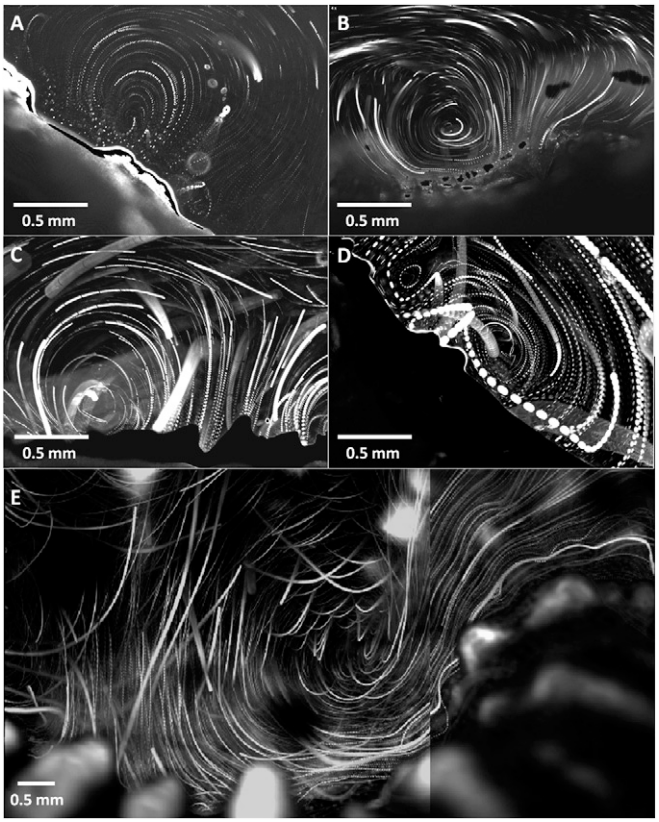

Fig. S2. Vortical flows near the surface of five additional coral species. (*A*) *S. pistillata*. (*B*) Unidentified *Acropora* sp. (*C*) Unidentified *Montipora* sp. (*D*) *S. hystrix*. (*E*) Composite image showing flow over a retracted polyp of an unidentified *Favia* sp. All panels are maximal intensity projections from videos. *A*–*D* were captured by dark-field microscopy using a 4× objective, with coral fragments held in a chamber similar to that used for microelectrode measurements. *E* was captured by epifluorescence microscopy using a 2× objective, with fluorescent beads used as tracer particles.

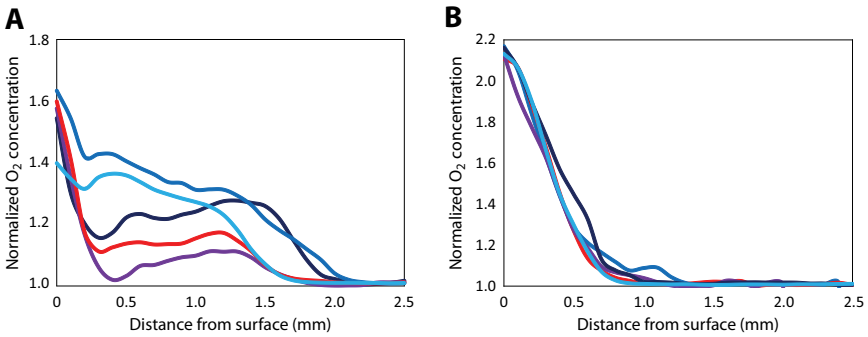

Fig. S3. Oxygen profiles near the surface of *P. damicornis* fragments (*A*) when cilia are beating and (*B*) when they are not. Profiles were measured perpendicular to the coral surface and normalized by the ambient oxygen concentration. In each case, five profiles obtained at different locations on different coral fragments are shown. In *B*, ciliary beating was arrested by the addition of 0.1 mM sodium-orthovanadate (*SI Materials and Methods*).

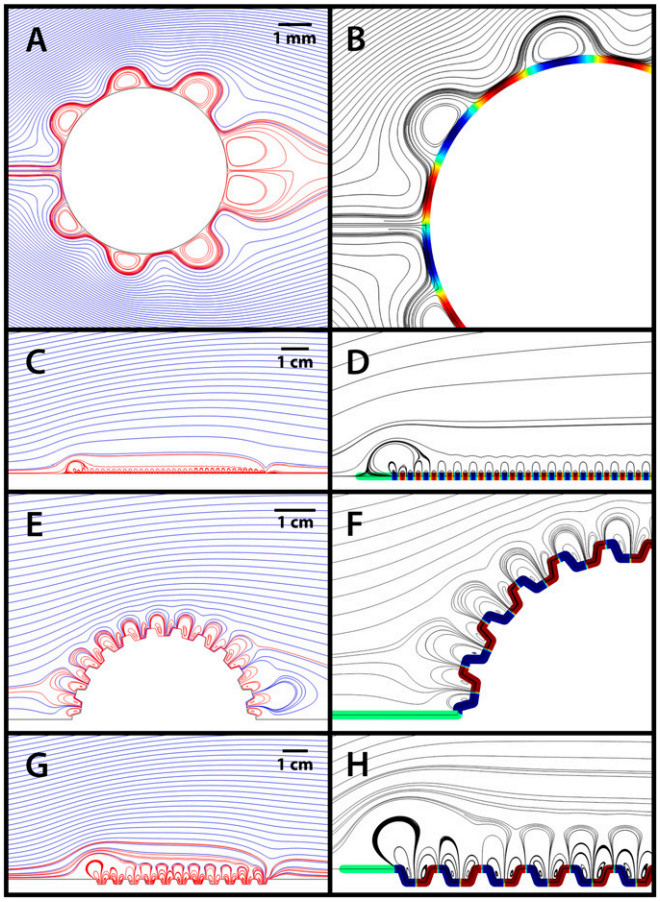

Fig. S4. Numerical simulations of ciliary flows in the presence of ambient flow for four different coral geometries. (*A* and *B*) Small-polyped branch. (*C* and *D*) Small-polyped plating colony. (*E* and *F*) Mounding large-polyped colony. (*G* and *H*) Large-polyped encrusting colony. *A*, *C*, *E*, and *G* show streamlines, with lines passing next to the coral surface or inside the cavities marked in red. *B*, *D*, *F*, and *H* show close-ups of *A*, *C*, *E*, and *G*, respectively, where streamlines are depicted in black and the ciliary forcing is denoted in color (red is to the right or clockwise, blue is to the left or counterclockwise, and green indicates a no-slip boundary condition). In *F*, the entire surface on both sides of the mound is no-slip. For all four geometries, the case is shown for which the Reynolds number [based on (*A* and *E*) diameter or (*C* and *G*) length as well as ambient flow velocity] is 10.

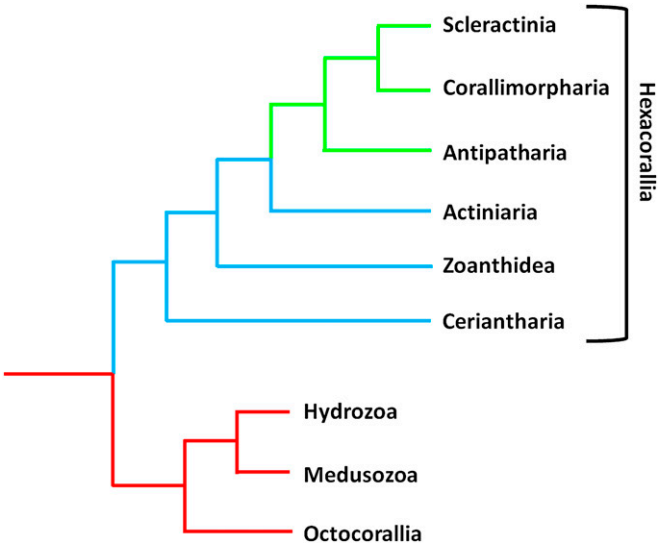

Fig. S5. Motile epidermal cilia in Cnidarian evolution. Presence/absence of epidermal cilia is overlaid on a schematic representation of phylogenetic relationships between different cnidarian groups based on molecular analysis (1–3). Colors denote groups in which the coral epidermis is fully ciliated (green), unciliated (red), or partially ciliated (blue; cilia confined to tentacles and oral discs) as detailed in Table S1.

1. Park E, et al. (2012) Estimation of divergence times in cnidarian evolution based on mitochondrial protein-coding genes and the fossil record. *Mol Phylogenet Evol* 62(1): 329–345.
2. Kayal E, Roure B, Philippe H, Collins AG, Lavrov DV (2013) Cnidarian phylogenetic relationships as revealed by mitogenomics. *BMC Evolutionary Biology* 13:5.
3. Berntson EA, France SC, Mullineaux LS (1999) Phylogenetic relationships within the class Anthozoa (phylum Cnidaria) based on nuclear 18S rDNA sequences. *Mol Phylogenet Evol* 13(2): 417–433.

Table S1. Presence/absence of epidermal cilia in different cnidarian species

Source	Objective	Main findings
Yonge (1)	Feeding behavior was studied in 40 GBR species of scl. corals in 15 different families as well as 2 species of octocorals	Ciliary flows observed in all scl. Corals; ectoderm thickly ciliated; ciliary flows mostly attributed cleansing role; occasionally also transport of food to the mouth; a general lack of ciliation of the ectoderm is noted for octocorals
Lewis and Price (2, 3)	Feeding behavior (2) and ciliary flows (3) were studied in 35 Atlantic species of scl. corals in 10 different families, mostly collected in Barbados, West Indies	Ciliary flows observed in all species; no ciliary reversal is observed; some evidence to support the involvement of ciliary flows in transporting food to the mouth; ciliary flows, hence, attributed mostly cleansing roles
Lewis (4)	Feeding behavior was studied in three species of black corals (*Antipatharia)* collected in Barbados	Colonies uniformly ciliated, similar to scl. corals; ciliary flows are generally directed toward the mouth; flow velocity seems to increase in the presence of food, suggesting involvement in feeding processes
Lewis (5)	Feeding behavior was studied in 30 species of octocorals in four families collected from GBR or Barbados	No ciliary flows observed except around the mouth and within the pharynx
Stafford-Smith and Ormond (6) and Stafford-Smith (7)	Sediment rejection mechanisms were studied in 42 GBR species of scl. corals belonging to 31 genera	Ciliary flows were observed in all species; for some species, cilia are important for removing sediments, particularly for sand or fine silt; however, many species (including *P. damicornis*) do not seem to depend on cilia for this function
Mariscal and Bigger (8)	EM study of the epithelial surface of scl. corals and octocorals	Surface of scl. corals is densely ciliated, whereas in octocorals, cilia are only found around the mouth
Eppard et al. (9)	EM study of the epithelial surface of the sea anemone *Acontiophorum niveum*	Cilia cover the tentacles and oral disk but are absent from the column
Martin et al. (10)	EM study of the metamorphosis of the hydrozoan *Mitrocomella polydiademata*	Epidermal cilia are found in the planula but lost in subsequent stages
Chia and Crawford (11)	EM study of planula and primary polyp of the sea pen *Ptilosarcus gurneyi*	Epidermal cilia are found in the planula but lost in the adult stage
Boelsterli (12)	EM study of early developmental stages in the anthomedusa *Podocoryne carnea*	Rudimentary nonfunctional cilia are formed during transdifferentiation and later disappear
Fautin and Mariscal (13)	EM study of the coralliimorpharian *Corynactis californica*	Motile cilia are found at different densities on different parts of the surface; attributed possible cleaning or feeding roles
This study (additional experiments)	Microscopic observation of ciliary flows on a polyp of *Discosoma* sp.	Ciliary flows were observed over the entire polyp, both above and below the disk surface, generally moving away from the mouth but forming local vortices around pseudotentacles
This study (additional experiments)	Microscopic observation of ciliary flows on polyps of two zoanthids *Protopalythoa* sp. and *Palythoa* sp.	Ciliary flows on the oral disk moving away from the mouth; little or no ciliary flows observed on tentacles

GBR, Great Barrier Reef; scl., scleractinian.

1. Yonge CM (1930) Studies on the physiology of corals. I. Feeding mechanisms and food. *Great Barrier Reef Expedition 1928-29, Scientific Reports* [British Museum (Natural History), London, UK], pp 13–57.
2. Lewis JB, Price WS (1975) Feeding mechanisms and feeding strategies of Atlantic reef corals. *J Zool* 176(4):527–544.
3. Lewis JB, Price WS (1976) Patterns of ciliary currents in Atlantic reef corals and their functional significance. *J Zool* 178(1):77–89.
4. Lewis JB (1978) Feeding mechanisms in black corals (antipatharia). *J Zool* 186(3):393–396.
5. Lewis JB (1982) Feeding behaviour and feeding ecology of the octocorallia (coelenterata: Anthozoa). *J Zool* 196(3):371–384.
6. Stafford-Smith M, Ormond R (1992) Sediment-rejection mechanisms of 42 species of Australian scleractinian corals. *Aus J Mar Fresh Res* 43(4):683–705.
7. Stafford-Smith M (1993) Sediment-rejection efficiency of 22 species of Australian scleractinian corals. *Mar Biol* 115(2):229–243.
8. Mariscal RN, Bigger CH (1977) Possible ecological significance of octocoral epithelial ultrastructure. *Proc 3rd Int Coral Reef Symp*, pp 127–133.
9. Eppard RA, Highison GJ, Mead RW (1989) Scanning electron microscopy of epithelial surfaces of the sea anemone *Acontiophorum niveum* (phylum cnidaria): Class anthozoa. *J Morphol* 200(1):63–69.
10. Martin V, Chia F, Koss R (1983) A fine structural study of metamorphosis of the hydrozoan *Mitrocomella polydiademata*. *J Morphol* 176(3):261–287.
11. Chia F, Crawford B (1977) Comparative fine structural studies of planulae and primary polyps of identical age of the sea pen, *Ptilosarcus gurneyl*. *J Morphol* 151(1):131–157.
12. Boelsterli U (1977) An electron microscopic study of early developmental stages, myogenesis, oogenesis and cnidogenesis in the anthomedusa, *Podocoryne carnea* M. Sars. *J Morphol* 154(2):259–289.
13. Fautin DG, Mariscal RN (1991) Cnidaria: Anthozoa. *Microscopic Anatomy of Invertebrates*, eds Harisson FW, Ruppert EE (Wiley-Liss, Hoboken, NJ), Vol 2, pp 267–358.

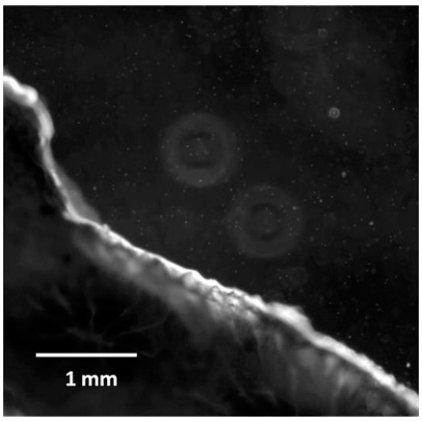

Movie S1. Ciliary flow on a *P. damicornis* fragment. The video shows vortical ciliary flows traced out by 1-μm particles suspended in the seawater adjacent to the coral fragment. A slightly zoomed-in view of the same location is seen in Fig. S1*B*. The video was captured by dark-field microscopy using a 4× objective at ∼30 frames per second and is played back at real time.

Movie S1

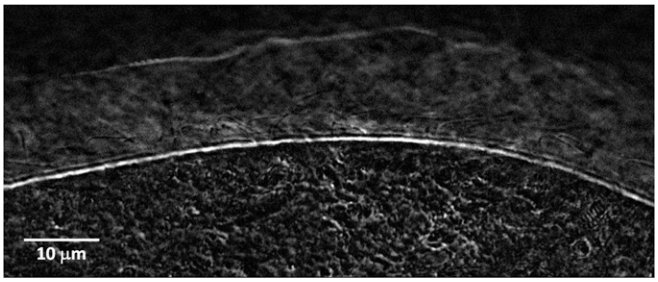

Movie S2. High-magnification imaging of beating cilia on the surface of a *P. damicornis* explant. The white contour is the edge of the coral tissue. Above it, cilia are clearly visible and beat mostly toward the right. The cilia beat rate was ∼16 Hz. The video was captured by phase-contrast microscopy using a 100× objective at 1,000 frames per second and is played back 33 times slower than real time.

Movie S2

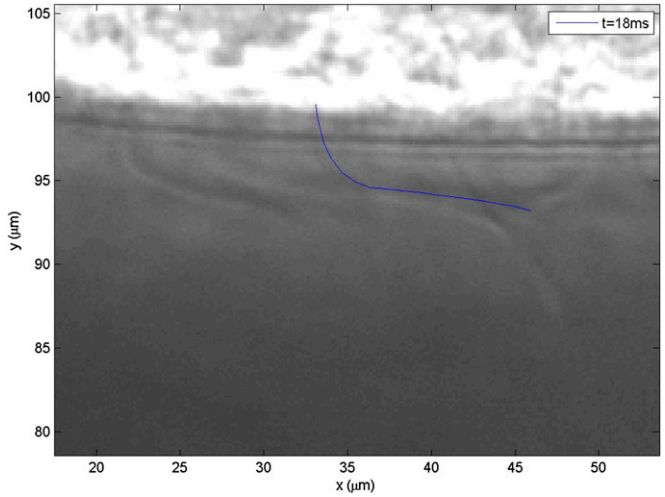

Movie S3. Tracking of a single coral cilium during a full beating cycle. The cilium was manually tracked in each frame using an in-house image analysis software written in Matlab (The MathWorks). The video was captured by phase-contrast microscopy using a 100× objective at 500 frames per second and is played back 86 times slower than real time.

Movie S3